Iranian Polymer Journal (2024) 33:405–418
https://doi.org/10.1007/s13726-023-01263-9

ORIGINAL RESEARCH

Inorganic particles/silica/polyacrylamide nanocomposite: as a potential application in water treatment

Fatemeh Salahi[1,2] · Amir Ershad-Langroudi[2] · Khadijeh Didehban[3]

Received: 28 May 2023 / Accepted: 31 October 2023 / Published online: 8 January 2024

Abstract

To develop an effective and novel adsorbent material consisting of three-layered core–shell particles with magnetic and photocatalytic properties, this study has utilized a sol–gel technique to synthesize $Fe_3O_4/SiO_2/TiO_2$/PAM (polyacrylamide) nanocomposite (FSTP NCs)-functionalized $Fe_3O_4/SiO_2/TiO_2$NPs as core and PAM as shell for water purification. The surface of the TiO_2 layer has been treated with silane A-174 (AA) as a coupling agent. In the final step, NPs were coated with PAM as an organic layer through radical polymerization of AA, to prepare a well-structured nanocomposite. FTIR, SEM, EDX, TEM, XRD, and VSM were applied to investigate the novel composed bonds, morphological properties of the surface and elemental analysis, core–shell structures, NPs size, samples phase and superparamagnetism of the NC and NPs, respectively. The R^2 values in three models of Langmuir (0.89), Freundlich (0.84), and Dubinin-Radushkevich (0.98) were calculated and the isotherm model followed a model with the highest R^2. The maximum efficiency of arsenate removal was recorded in 0.1 g concentration of adsorbent, pH 2, contact time of 700 min, and ion concentration of 50 mg/L.

✉ Amir Ershad-Langroudi
A.Ershad@ippi.ac.ir

[1] Department of Chemistry, Payame Noor University (PNU), P.O. Box, Tehran 19395-4697, Iran

[2] Color and Surface Coating (CRSC) Department, Polymer Processing Faculty (PPF), Iran Polymer and Petrochemical Institute (IPPI), Tehran 14965/115, Iran

[3] Department of Chemistry, Payame Noor University (PNU), P.O. Box, Tehran 19395-36972, Iran

Graphical abstract

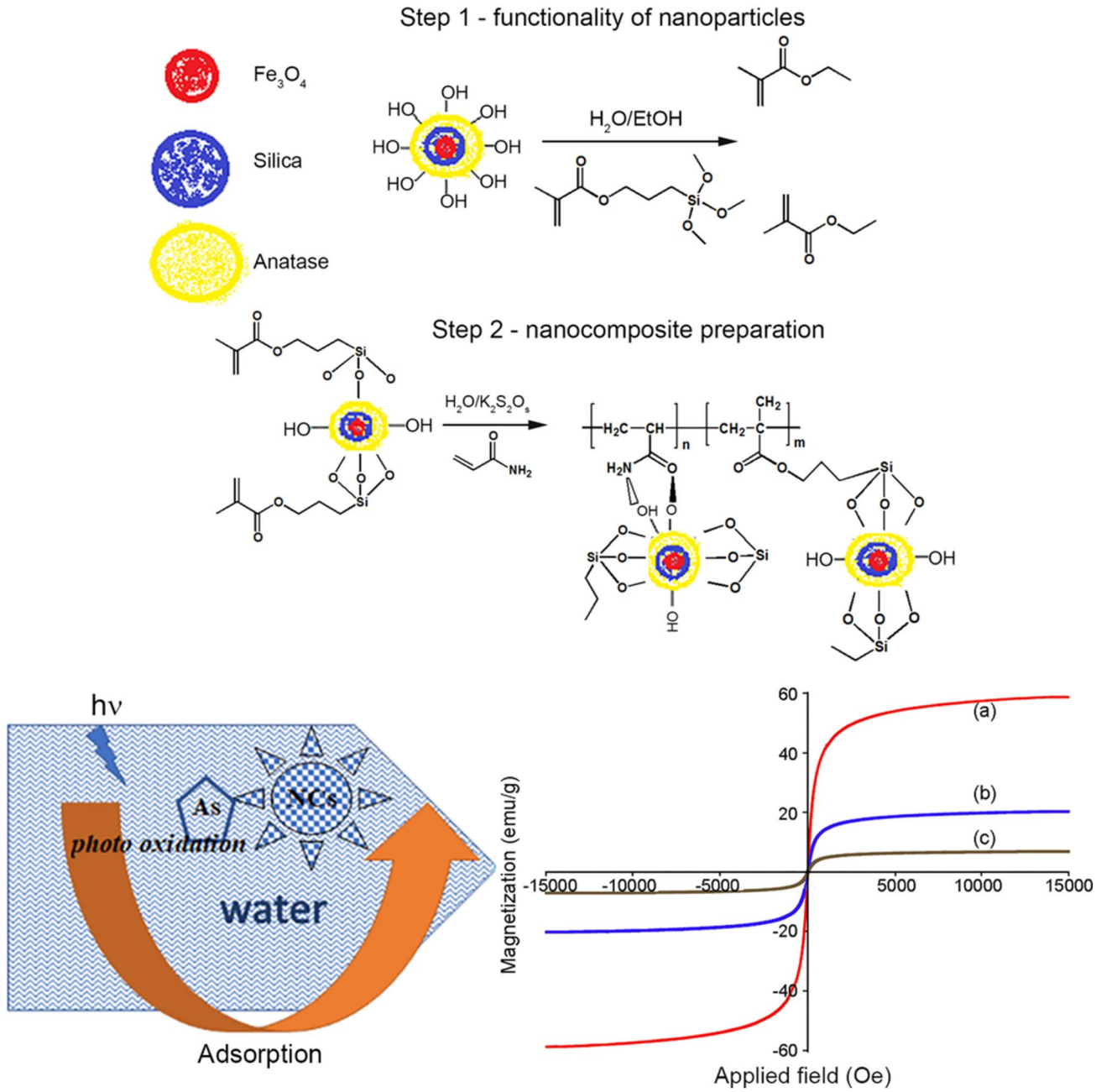

Keywords Polyacrylamide · Nanoparticles · Magnetite · Photodegradation · Water purification · Coupling agent

Introduction

Regularly, a wide variety of chemicals with detrimental effects on the environment are found in water. Although water is often taken for granted, it is undoubtedly one of nature's most precious gifts. However, with increasing population, desertification, deforestation, and other ages of industrialization legacies, the demand for water resources has increased exponentially [1–3]. The potential adverse effects of arsenic-contaminated water on human health are a matter of significant concern. It should be noted that approaches only focused on reducing the arsenic content to a level of 10 parts per billion (ppb) may not provide a comprehensive solution. Hence, professionals and governmental

authorities place significant importance on this matter [4–6]. Water contaminants such as organic and inorganic pollutants have critical consequences on human health and even the ecosystem [7, 8]. In recent decades, various methodologies have been investigated for water purification [9–11]. The imperative need to reduce the pollutant content of wastewater necessitates the use of technologically advanced solutions that prioritize high efficiency and cost-effectiveness while adhering to principles of sustainable and environmentally friendly practices [12, 13].

Polymeric nanocomposites have been taken into consideration in chemistry, material science, catalyst, biomaterial, etc., due to their significant properties such as mechanical, thermal, optical, and electrical properties, and also improve flexible processability [14, 15]. Many factors influence these properties such as the size and concentration of inorganic nanofiller materials, as well as their interactions with a polymer matrix [16–18]. One of the most applicable methods for the synthesis of polymeric nanocomposites is the sol–gel method which has been applied in different applications [19, 20]. The molar ratio of reactants, concentration, temperature, time, and pH play vital roles in the sol–gel method [21–23].

Among several applicable NPs, magnetite iron oxide NPs have spectacular performances (perform strikingly) [24–26]. There are various forms of iron oxides, such as goethite, amorphous, and crystalline ferric oxide [27]. Magnetite iron oxide NPs were selected for assorted goals, including water and air purification [28, 29], removal of metal ions [30, 31], cancer therapy, magnetic resonance imaging, drug delivery systems, catalyst, and magnetic sensing [32]. In the world of irretrievable (irrecoverable) materials, magnetite iron oxide NPs are readily degradable [33, 34]. Besides other significant advantages like high biocompatibility, availability, low cost, large surface area, and large surface-free energy, a double-edged sword, they easily aggregate [35]. As the high surface energy was responsible for the aggregation of Fe_3O_4 NPs, reducing the surface energy is a challenging issue. Surface modification with surfactants, coupling agents, and organic ligands can solve the problem [36–38].

Silane groups are widely used modifiers in many applications owing to their favorable attributes such as biocompatibility, biosafety, accessibility, facile surface modification, cost-effectiveness, and convenient regulation of interparticle interactions. Silica has been acknowledged as a secure substance that has potential for utilization within the pharmaceutical sector [39]. Over the last decade, silica coatings have attracted intense attention in water remediation [40]. Because of the open-pore structures, pore size distribution, large pore volume, and high surface, it could be helpful in adopting industrial pollutants [40].

Nanocrystalline TiO_2 is an extraordinary (a prominent) multifunctional nanoparticle due to its inexpensiveness, availability, long-term stability, biocompatibility, nontoxicity, and photoactivity properties [41, 42]. Possessing remarkable capacity decomposition of many organic compounds from wastewater, antibacterial effect, and strong photo-catalytic reaction, titania is reported to opt for preparing nanocomposite for water purification purposes [43]. The photochemical activity of titania will be enhanced by doping or suppressing with metal ions such as nickel, zinc, iron, etc. [44, 45]. One of the most functional synthetic polymers in various applications is polyacrylamide (PAM). Anionic polyelectrolytes, of which acrylamide is one, are water-soluble polymers that carry a negative charge and are employed in a wide range of settings, including lubrication, wastewater restoration, mining, paper production, and water management. Hence, nanocomposites of this polymer have been extensively used as flocculants [46–48].

One of the most controversial issues in the study of nanomaterials is decreasing the surface energy to avoid agglomeration. Furthermore, NPs naturally possess high activity and are easily oxidized in the air, which reduces their magnetic properties. So, the surface modification should be a final remedy [49, 50]. It is noteworthy that the strength of the interaction between NPs and polymer matrix should be observed to prevent gas voids and destructive effects on nanocomposite characterization. Recently, several magnetic photocatalytic NCs have been synthesized. Yin et al. prepared (γ-Fe_2O_3 on SiO_2) on TiO_2 hybrid as a catalyst to degrade methylene blue [51]. Oxidation of oxalic acid in the presence of $Zn_{0.35}Ni_{0.65}Fe_2O_4/SiO_2/TiO_2$ NPs was carried out by Shchukin et al. [52]. Despite some advantages, such as a strong covalent bond, the methodology of grafting and polymerization of AA on the surface of TiO_2 NPs is still a challenge [53, 54].

The aim of this research is to illustrate a sol–gel method to construct a $Fe_3O_4/SiO_2/TiO_2$/PAM nanocomposite with a photocatalytic performance. The selection of Fe_3O_4 was chosen to impart magnetic properties to the particles. To construct the initial shell and prevent aggregation of the magnetite nanoparticles, TEOS and DEDMS were utilized as silane sources. The second shell was fabricated using titanium dioxide nanoparticles (TiO_2 NPs) due to their exceptional photocatalytic properties derived from the titania source. The attainment of the final shell was accomplished through the process of radical polymerization of acrylamide on the outermost surface of the preceding shell. Water purification has been examined for the removal of arsenic ions, although acrylamide and its derivatives are known in water treatment and industrial wastewater treatment. The novelty of this study lies in the development of a nanocomposite material composed of three-layered core–shell particles with both magnetic and photocatalytic capabilities. This nanocomposite is synthesized using acrylamide as a base material, which exhibits a porous structure suitable for the removal of hazardous metal oxides from water. Furthermore,

this material has the advantages of user-friendly application and facile separation. An additional contribution of this work is the examination of the behavior of the composite material used for the separation of 5-valent arsenic, using established isotherm and synthetic models for analysis. Thus, this well-established core–shell nanocomposite is versatile and could be applied in various fields such as water treatment, drug delivery, antibacterial effect, and catalyst.

Experimental

Materials and reagents

The deionized water (DI) utilized for all experiments was provided by aquaMAX-Basic 360 Series (Korea Made). All chemicals were of analytical grade and were used as received without any purification. Iron (III) chloride hexahydrate ($FeCl_3.6H_2O$), Iron (II) sulfate heptahydrate ($Fe_SO_4.7H_2O$), and acrylamide monomer (AA) were purchased from Merck. Potassium persulfate (KPS), *Tetra-n*-butyl *ortho*-titanate (TBOT, 97%), ammonium hydroxide (25% by weight), and hydrochloric acid (HCl, 37% by weight) were purchased from Merck, Sigma-Aldrich, Merck, and Merck, respectively. Tetraethyl *ortho*-silicate (TEOS, ≥ 98%) and diethoxy dimethylsilane (DEDMS), and silane A-174 were purchased from Merck, Sigma-Aldrich, and Sigma-Aldrich, respectively. Absolute ethanol (99.9%, Merck), acetylacetone (97%, Merck), and butanol (99%, Merck) were used as a solvent without further purification.

Preparation of Fe_3O_4 NPs

6.945 g (0.025 mol) of $FeSO_4.7H_2O$ and 13.45 g (0.05 mol) of $FeCl_3.6H_2O$ were dissolved in 500 mL of deionized water (DW) at (60–70 °C) temperature. Subsequently, to establish the desired pH range of 9–11 and induce the precipitation of magnetite, the ammonia solution with a concentration of 25% was gradually introduced in the form of drops. After the completion of the reaction, the resultant was filtrated and washed with DI and then put into an oven at 60 °C for 24 h [49].

Preparation of Fe_3O_4/SiO_2 NPs

Fe_3O_4 NPs of 0.44 g were dispersed under sonication in a mixture of ammonia/water/ethanol. A solution of TEOS in ethanol and diethoxydimethylsilane was added gradually into the mentioned suspension under mechanical stirring (140 rpm), and the hydrolysis continued for 8 h. The resultant was separated with a magnet, washed three times with ethanol, and dispersed in ethanol for use [49].

Preparation of TiO_2 NPs

First of all, TBOT was dissolved in butanol under magnetic stirring. Then acetylacetone (as a chelating agent to control the rate of hydrolysis and condensation reactions) was added and the mixture was stirred at ambient temperature [20]. The molar ratio of TBT/EAcAc/butanol was 1:1:20. The hydrolysis began by adding TiO_2 (anatase) and was prepared by 8 h reflux of the sol at 80 °C [20].

Preparation of $Fe_3O_4/SiO_2/TiO_2$ NPs

The prepared TiO_2 nanoparticle sols and a certain amount of iron chloride (to transfer into visible light range) were added to the dispersed Fe_3O_4/SiO_2 suspension dropwise under 16 h vigorous stirring with water reflux and aged for 24 h [43, 55].

Preparation of $Fe_3O_4/SiO_2/TiO_2$/PAM NC

First of all, to increase surface attaching capacity, the surface of magnetite/silica/TiO_2particle was functionalized by silane A-174 which was carried out on TiO_2 surface as the outer surface. The magnetite/silica/TiO_2 nanocomposite was added to a mixture containing silane A-174, H_2O, and ammonium hydroxide (25% by weight). The combination was sonicated for 10 min and then stirred for 3–4 h at (70–80 °C) temperature. Second, a solution of 10% (by weight) of acrylamide under a nitrogen atmosphere was prepared. The modified nanocomposite and potassium persulfate (with a ratio of 1000:1) were mixed under the nitrogen atmosphere and then added to the reaction vessel. Then, acrylamide was polymerized under an N_2 atmosphere and constant stirring at 75 ± 5 °C for 4 h [43, 55]. Ultimately, the white viscous solution was cooled at room temperature. The product was first purified using MeOH, and then by dissolving in water and ethanol three times. Scheme 1 signifies the various steps of nanocomposite synthesis.

Arsenic removal

The effectiveness of the nanocomposite in removing arsenate (V) from an aqueous solution was used to assess its potential for use in water purification. Nanocomposite samples (typically 0.1 g) were introduced directly to aqueous solutions of varying arsenic (V) concentrations. After a 12 h incubation period, the nanocomposite was magnetically extracted. The arsenic content in the supernatant was analyzed by inductively coupled plasma (ICP) [49]. To find the effect of the pH solution, pH was adjusted between 2 and 7. Also, the results of the amount of adsorbent, contact time, and ion concentration were studied. Here, isotherm and kinetic models were applied [56].

Scheme 1 Various steps of nanocomposite synthesis

Characterization

Fourier transform infrared (FTIR) spectra of the samples were recorded as KBr pellets on an FT-IR Equinox 55 spectrophotometer in the range of 4000–400 cm^{-1}. The morphological properties of the surface of the gold-coated samples were investigated using scanning electron microscopy (SEM) on a Cambridge S360 microscope at 20 kV and 2.85 A probe current. The EDX spectroscopy was performed by SEM–EDX mapping (LEO 440) to investigate elemental analysis. Using TGA/DSC1, Mettler Toledo (Switzerland) thermal stability and the amount of inorganic content of

hybrid nanocomposites were studied under nitrogen flow at a heating rate of 10 °C/min. Transmission electron microscopy (TEM) provided data on the particle shapes, sizes, and thickness of the modified layers on the surface of NPs. The TEM image was obtained by Philips EM 208, H-7100. The phases of the samples were identified by X-ray diffraction (XRD) Siemens, D5000 X-ray diffractometer at room temperature. The magnetic feature of NPs was examined using a vibrating sample magnetometer (VSM) made by Daghigh Kavir Corporation.

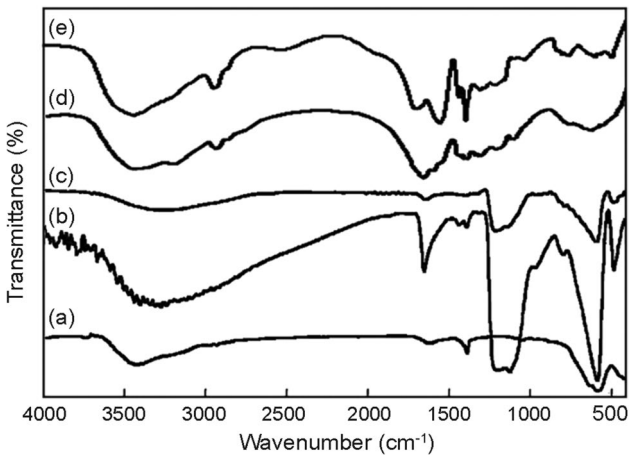

Fig. 1 FTIR spectra of: (**a**) Fe_3O_4, (**b**) Fe_3O_4/SiO_2, (**c**) $Fe_3O_4/SiO_2/TiO_2$, (**d**) PAM, and (**e**) $Fe_3O_4/SiO_2/TiO_2$/PAM

Results and discussion

FTIR analysis

To scrutinize the interface bonding in the $Fe_3O_4/SiO_2/TiO_2$/PAM NC, the FTIR spectrum of samples 1 to 5 was measured and indicated in Fig. 1a–e. In all spectra, the wavenumber around 570–590 cm^{-1} represents the characteristic Fe–O bending vibration in magnetite [49]. In Fig. 1b, the stretching vibrations at around 1100–1150, 950, 805, and 500–600 cm^{-1} are related to Si–O–Si, Si–OH, Si–O, and bending of Si–O, respectively. The presence of the Fe–O–Si band at around 1050 cm^{-1} indicates that the sample has sufficiently SiO_2 doping [57]. In Fig. 1c, characteristic peaks of TiO_2 were overlapped with the Fe_3O_4 and SiO_2 but the intensity of this spectrum was lowered meaning the coverage of $Fe_3O_4/SiO_2$by TiO_2 [41]. In the spectrum of PAM (Fig. 1d), vibrations of C = O happened at 1703 cm^{-1}. Bending vibrations of hydrogen in CH_2 and vinyl groups appeared at 1452 and 1407 cm^{-1}, respectively [58]. Stretching vibration of C–H was recorded at 2950 cm^{-1}. In the spectrum of $Fe_3O_4/SiO_2/TiO_2$/PAM NC (Fig. 1e), bands at around 570 and 1600 cm^{-1} might belong to the $Fe_3O_4/SiO_2/TiO_2$ NPs, which were absent in the spectrum of PAM (Fig. 1d). Scheme 2 shows the proposed schematic presentation for two steps of nanocomposite preparation as well as hydrogen bonding between the OH groups of the modified Fe_3O_4/

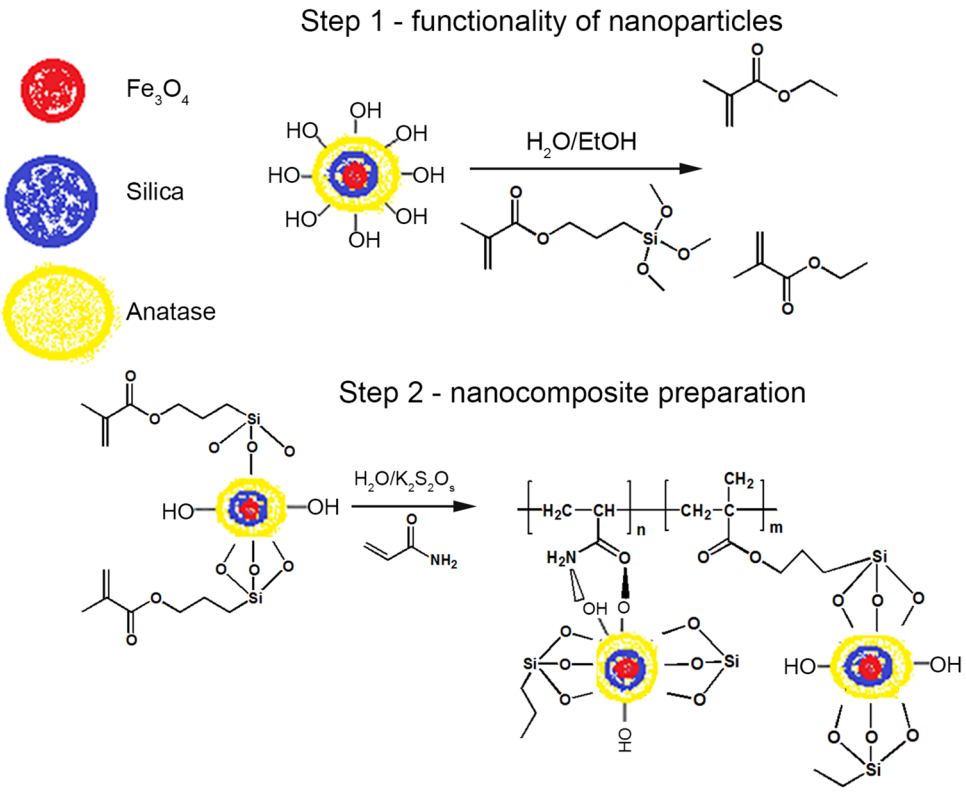

Scheme 2 Schematic presentation for 2 steps of nanocomposite preparation and hydrogen bonding

SiO_2/TiO_2 NPs and amide groups of the acrylamide in the nanocomposite [43].

XRD analysis

In the XRD pattern of Fe_3O_4 NPs, crystal planes (220), (311), (400), (422), (511), and (440) of Fe_3O_4 NPs appeared at 30.0°, 35.4°, 43.0°, 53.6°, 57.2°, and 62.5°, respectively [59]. Using Scherrer's equation (Dhkl = 0.89λ/(βcosθ), where β is the width of the XRD peak at the half-peak height, λ is the X-ray wavelength in nanometers, and θ is the half diffraction angle of 2θ in degrees). The average crystallite size of Fe_3O_4 was calculated using Scherrer's formula and from D311, which was around 12 nm [60]. The diffraction pattern of Fe_3O_4/SiO_2 nanoparticles (Fig. 2b) reveals the presence of a semi-crystalline structure of SiO_2, as well as the observation of diffraction peaks corresponding to Fe_3O_4. This observation provides confirmation of the successful production of Fe_3O_4/SiO_2 [61]. Following the encasing of Fe_3O_4/SiO_2 with TiO_2 (as seen in Fig. 2c), a distinct peak emerged at about 25°, signifying the occurrence of anatase phase development [62, 63]. Upon the integration of $Fe_3O_4/SiO_2/TiO_2$into PAM, diffraction patterns of the nanofiller were seen (as shown in Fig. 2d). This observation indicated that the incorporation procedure failed to have a noticeable effect on the structure of the nanofiller.

EDX analysis and SEM

To ascertain the presence of the constituents of the nanofiller PAM, analytical techniques including EDX and elemental mapping were used (Fig. 3). As seen in the EDX spectrum, Fe, Si, and Ti were well characterized, and according to the elemental mapping, they were uniformly dispersed into PAM. Furthermore, the SEM image of $Fe_3O_4/SiO_2/TiO_2$ and $Fe_3O_4/SiO_2/TiO_2$/PAM are shown in Fig. 4. It is evident that $Fe_3O_4/SiO_2/TiO_2$ has a porous structure, as seen in (Fig. 4a), and, when embedding in PAM, the resulting material also retains its porous nature (Fig. 4 b). This porous structure makes the nanocomposite potent for the adsorption process.

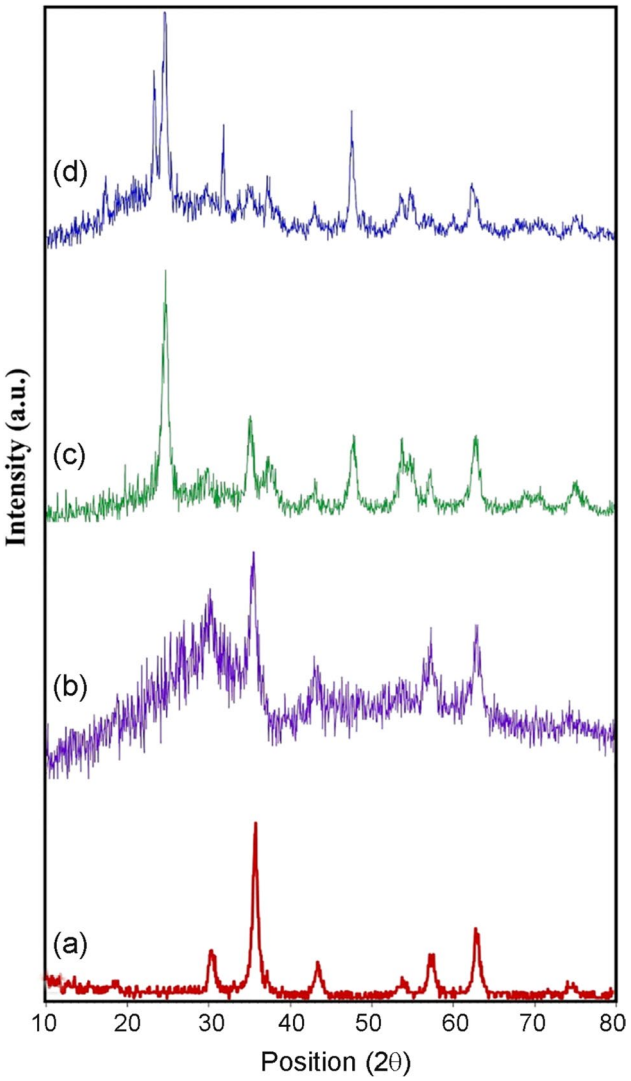

Fig. 2 XRD patterns of: (**a**) Fe_3O_4, (b) Fe_3O_4/SiO_2, (**c**) $Fe_3O_4/SiO_2/TiO_2$, and (**d**) $Fe_3O_4/SiO_2/TiO_2$/PAM

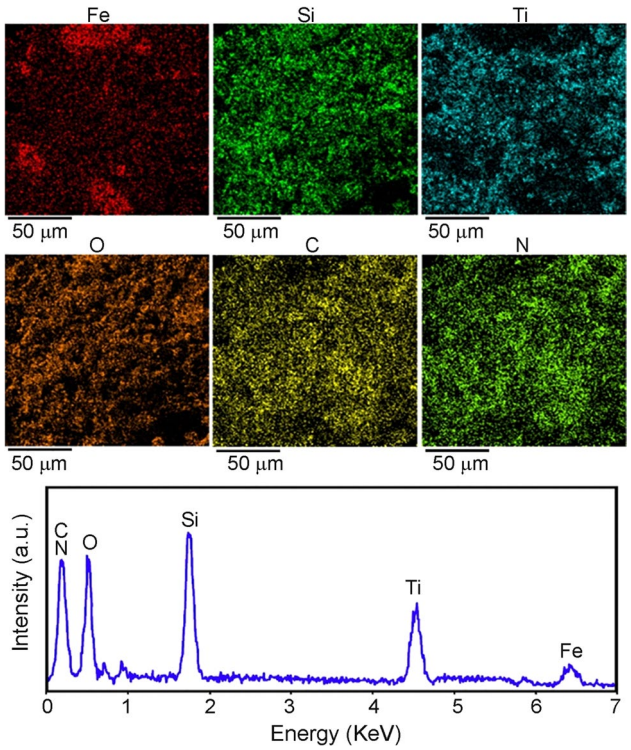

Fig. 3 EDX spectrum and elemental mapping of $Fe_3O_4/SiO_2/TiO_2$/PAM NCs

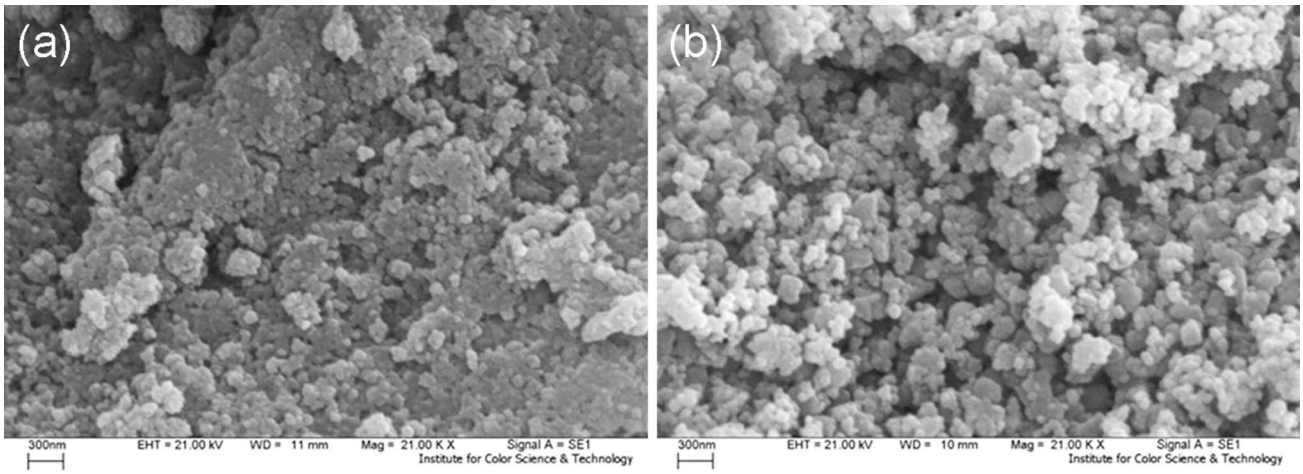

Fig. 4 FE-SEM images of: (**a**) $Fe_3O_4/SiO_2/TiO_2$, and (**b**) $Fe_3O_4/SiO_2/TiO_2$/PAM

TEM imaging

To examine the morphology, dimensions, and distribution of produced nanoparticles, transmission electron microscopy (TEM) was used. Figure 5 presents the visual representations of $Fe_3O_4/SiO_2/TiO_2$ and $Fe_3O_4/SiO_2/TiO_2$/PAM. $Fe_3O_4/SiO_2/TiO_2$ (Fig. 5a) illustrates the polygonal particles with a size of less than 40 nm. The TEM imagine shown in Fig. 5b reveals that the $Fe_3O_4/SiO_2/TiO_2$ particles are enveloped by a layer of polyacrylamide (PAM). This image provides evidence of a favorable distribution of the nanofiller inside the PAM matrix, corroborating the results obtained from elemental analysis [64, 65].

Vibrating sample magnetometer (VSM)

Vibrating sample magnetometry (VSM) is a very effective methodology used for the examination of magnetic characteristics in various materials, including those pertaining to water treatment and the elimination of arsenate. The use of VSM enables the examination of the magnetic properties of the adsorbents before to and subsequent to the adsorption of arsenate. This analytical technique aids in discerning whether the adsorption process is driven by magnetic interactions or other processes, such as surface complexation or ion exchange. The magnetic characteristics of Fe_3O_4 and $Fe_3O_4/SiO_2/TiO_2$ NPs and $Fe_3O_4/SiO_2/TiO_2$/PAM NC were examined using VSM analysis (Fig. 6). For Fe_3O_4 NPs, a superparamagnetic behavior was observed, and the residual and saturation magnetizations and coerciveness were 1.6 and 67.7 emu/g, and zero, respectively. $Fe_3O_4/SiO_2/TiO_2$ NPs had residual and saturation magnetizations of 0.74 and 16.7 emu/g, as well as coerciveness of 5.78 Gs. These NPs still have superparamagnetic features.

Using BET analysis, the surface area of $Fe_3O_4/SiO_2/TiO_2$/PAM was calculated as 40.5 m^2/g, which would be suitable for the adsorption process.ε2 C_e/q_e.

Arsenate removal

Given the recent implementation of stricter drinking water regulations by the World Health Organization (WHO), which now limits the acceptable level of arsenic to 10 µg/L, there is a pressing need to identify effective sorbent materials

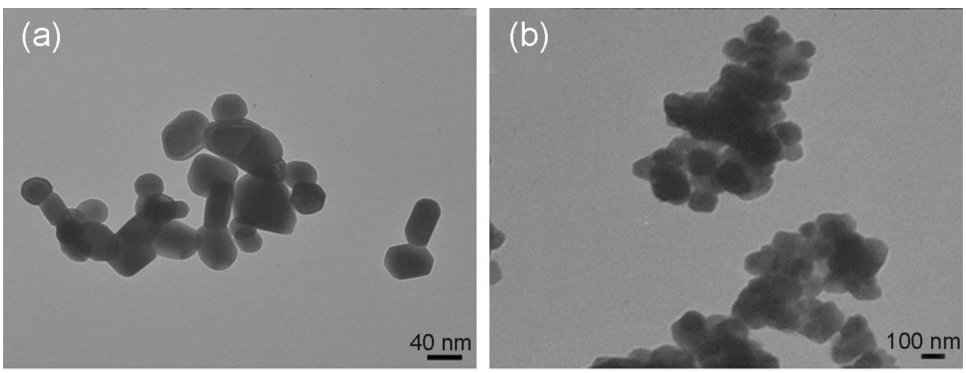

Fig. 5 TEM images of:(**a**) $Fe_3O_4/SiO_2/TiO_2$, and (**b**) $Fe_3O_4/SiO_2/TiO_2$/PAM

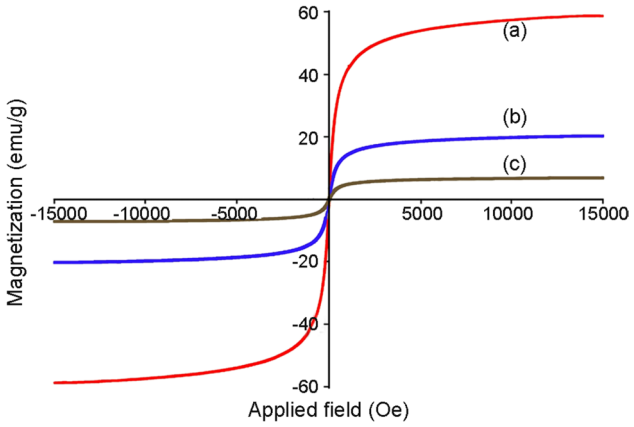

Fig. 6 Magnetization curves of: (**a**) Fe_3O_4, (**b**) $Fe_3O_4/SiO_2/TiO_2$, and (**c**) $Fe_3O_4/SiO_2/TiO_2$/PAM

capable of efficiently removing arsenic from water sources. The efficiency of adsorption in a certain adsorbate-adsorbent system exhibited a direct proportionality to the concentration of the adsorbent. This correlation can be attributed to the presence of several unoccupied binding sites. Additionally, the adsorption process reached equilibrium rapidly. The process of arsenic adsorption exhibits a fast rise, eventually reaching a state of equilibrium when a saturation plateau is seen. This plateau is a result of the binding sites on the surface of the adsorbent being fully occupied. Figure 7a shows the effect of the amount of the adsorbent on the removal efficiency. As can be seen, by increasing the amount of adsorbent, the removal efficiency was increased. In a high amount of adsorbent, some aggregations may occur, and this leads to a decrease in removal efficiency. Thus, 0.1 g was chosen as the optimum amount of adsorbent. The effect of changing the pH of the solution was shown in Fig. 7b. Iron oxide has surface OH groups that undergo protonation or deprotonation in response to the pH level of the solution. With increasing the pH, the surface of the adsorbent became more hostile, and caused an electrostatic repulsion with negatively charged ions. To illustrate, the decrease in adsorption capacity seen at elevated pH levels may be ascribed to the electrostatic repulsion occurring between the arsenite anion and the negatively charged surface of the adsorbent. Therefore, at pH 2, maximum efficiency occurred (around 55%). Contact time is another crucial factor. The effectiveness of the process is significantly affected by the duration of contact between the adsorbate and adsorbent. A shorter time required to reach adsorption equilibrium indicates a more rapid removal of arsenic (As) within fewer time intervals. The effect of contact time on the adsorption process is depicted in Fig. 7c. As seen, at first, the adsorption rate is fast and the equilibrium occurred after about 700 min. The effect of ions concentration on the adsorption process is illustrated in Fig. 7d. As can be seen, increasing the concentration up to 50 mg/L, led to an increase in removal efficiency (as maximum efficiency). The efficacy of arsenic removal may decrease when the ion concentration is high, especially in the presence of competing ions. This phenomenon occurs due to the competitive nature of these ions, as they compete for the few adsorption sites present on the adsorbent material, hence diminishing the efficacy of arsenite removal. Lower values of ion concentration have the potential to augment the adsorption capacity of the adsorbent material, hence facilitating a more efficient elimination of arsenic from the solution.

To find the relationship between the adsorbent and adsorbate, isotherm models [66]were applied, and the plots and results are shown in Fig. 8 and Table 1, respectively.

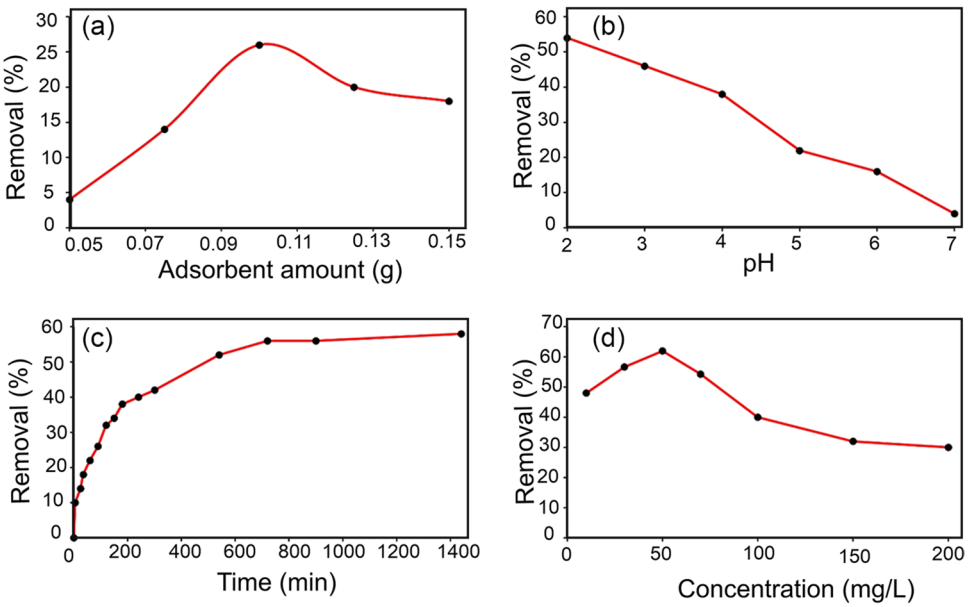

Fig. 7 Effects of: (**a**) adsorbent amount, (**b**) solution pH, (**c**) time, and (**d**) ion concentration on the adsorption process

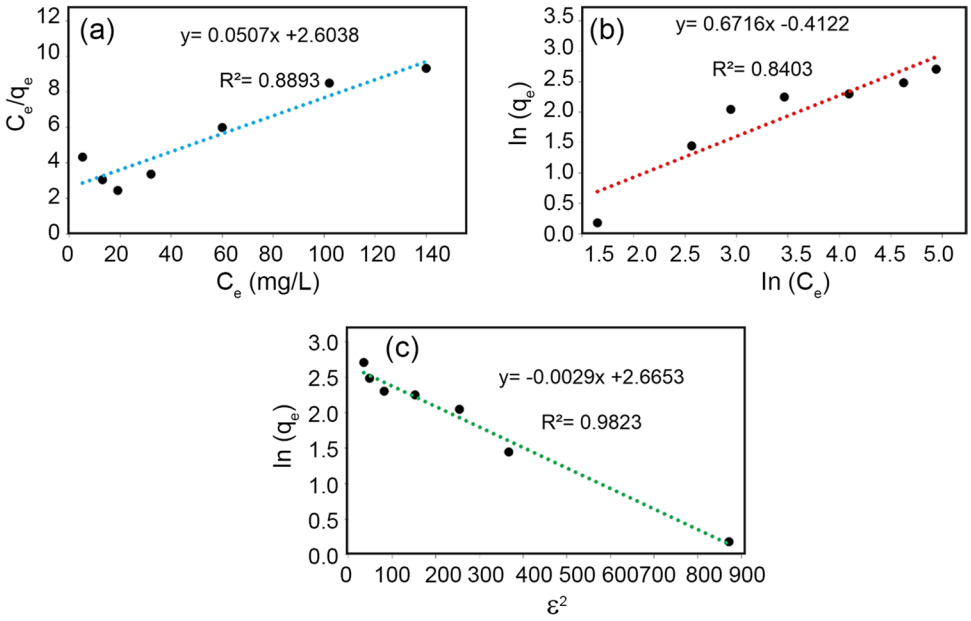

Fig. 8 Plots of: (**a**) Langmuir, (**b**) Freundlich, and (**c**) Dubinin-Radushkevich isotherm models

Table 1 Isotherm equations and the obtained parameters

Isotherm models	Equations	Parameters
Langmuir	$C_e/q_e = 1/K_L.q_m + C_e/q_m$	$q_m = 20$ mg/g, $K_L = 0.02$ (L/mg), $R^2 = 0.89$
Freundlich	$\ln q_e = \ln K_F + 1/n_F \ln C_e$	$K_F = 0.66$ (L/g), $n_F = 1.50$, $R^2 = 0.84$
Dubinin-Radushkevich	$\ln q_e = \ln q_m - B_{D\text{-}R}[RT\ln(1 + 1/C_e)]^2$	$q_m = 14$ mg/g, $K_{D\text{-}R} = 0.003$ (mol^2/J^2), $R^2 = 0.98$

C_e = Concentration of adsorbate (mg/L)
q_e = Adsorption capacity in the equilibrium state (mg/g)
q_m = Maximum adsorption capacity (mg/g)
K_L = Langmuir constant (g/mg)
K_F = Freundlich constant (L/g)
n_F = Sorption intensity
q_D = Maximum sorption capacity (mg/g)
B_D = Dubinin-Radushkevich constant (mol^2/kJ)
R = Ideal gas constant (8.314 J/(Kmol))
T = Absolute temperature (K)

The coefficient of determination (R^2 value) serves as a metric for evaluating the degree to which a model fits the observed data. The DRK model often exhibits a greater R^2 in comparison to other models when used on the same dataset. This finding suggests that the DRK model provides a more precise representation of the underlying adsorption behavior and exhibits a better agreement with the experimental data [67]. As seen in Fig. 8, the Dubinin-Radushkevich isotherm model, due to its higher amount of R^2, fits the experimental data better than other models. This isotherm model expresses a volume filling of micropores adsorption mechanism [68].

The findings obtained from the fitting of the kinetic experiments using the two models are summarized in Table 2 and Fig. 9. The kinetics is determined within an optimal time frame. The kinetic experimental data exhibit a strong agreement with both a pseudo-first order kinetic model ($R^2 = 0.9777$) and a pseudo-second order model ($R^2 = 0.9953$). The study of kinetics has significant intrigue for the potential use of this sorbent in the field of water treatment [69]. As can be inferred, the higher amount of R^2 for pseudo-second-order and closer the amount of $q_{e,\,cal}$ to the experimental value indicated that this model fits better the experimental data. Thus, it could be said that the primary interaction between arsenate and hydrogel is chemical (like electrostatic attraction).

Table 2 Kinetic equations and obtained parameters

Kinetic models	Equations	Parameters
Pseudo-first order	$\ln(q_e\text{-}q_t)=\ln q_e-K_1t$	$K_1=0.004$ (1/min), $q_{e,\,cal}=5.7$ (mg/g), $q_{e,\,exp}=7$ (mg/g), $R^2=0.98$
Pseudo-second order	$t/q_t=1/K_2.q_e^2+t/q_e$	$K_2=0.001$ (g/mg.min), $q_{e,\,cal}=7.7$ (mg/g), $q_{e,\,exp}=7$ (mg/g), $R^2=0.99$

q_e = Adsorption capacity at equilibrium (mg/g)
q_t = Adsorption capacity at different times (mg/g)
K_1 = Rate constant (1/min)
t = Contact time (min)
K_2 = Rate constant (g/(mgmin))

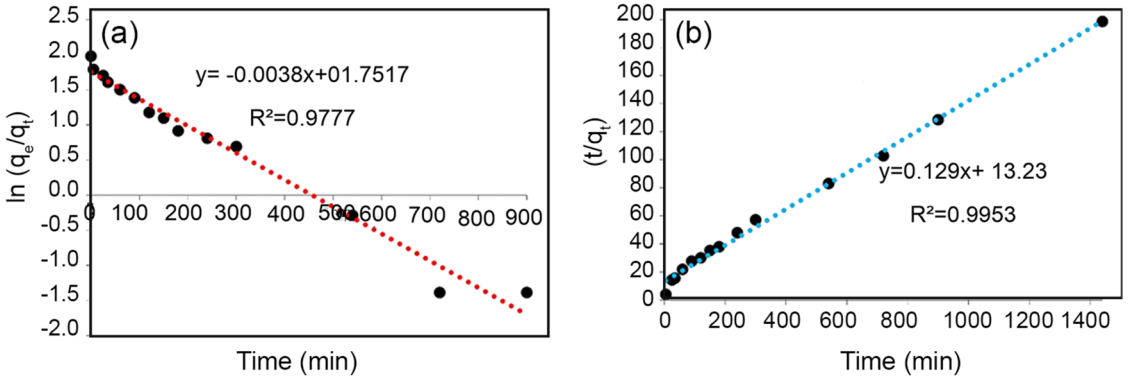

Fig. 9 Plots of: (**a**) pseudo-first-order, and (**b**) pseudo-second-order kinetic mod

Conclusion

The issue of water pollution has generated significant alarm among specialists. Consequently, an adsorbent was synthesized with the purpose of effectively eliminating arsenate from aqueous environments. The straightforward and sequential sol–gel process was implemented to produce the $Fe_3O_4/SiO_2/TiO_2$/PAM nanocomposite. The first step was the synthesis of magnetite nanoparticles by the chemical co-precipitation process, serving as the core material. TEOS and DEDMS were employed as silane sources to build the first shell and modify magnetite NPs to prevent their aggregation. The second shell was prepared by TiO_2 NPs due to their great photocatalytic character from TBOT as a source of titania. The ultimate shell was achieved by radical polymerization of AA on the surface of the last shell. However, it would not be attained without the surface functionalization of TiO_2 NPs with silane A-174. Silanes are essential in the preparation of FSTP NCs. The prepared FSTP NCs were verified using several analytical techniques, including FTIR spectroscopy, XRD, SEM–EDX, and TEM. The core–shell structure was seen through the application of SEM and TEM, which allowed for a layer-by-layer analysis. On one hand, the first shell serves to augment the stability of magnetite while concurrently heightening its photocatalytic characteristics. In contrast, the use of silane for the purpose of surface modification of TiO_2 NPs results in the formation of novel covalent solid bonds with AA monomers, leading to the establishment of a structured polymerized network of PAM. Water treatment tests were obtained through entrapment of molecules in the PAM network and chemical reactions through hanging PAM functional groups. As mentioned earlier, many other tests were applied to prove synthetic FSTP NCs structure. It will be expected that these sorts of fascinating superparamagnetic FSTP NCs with such an artistic frame open up the cleaner and green horizons of the world of tomorrow. Studies of isotherm and kinetic models revealed that the adsorption mechanism is a pore-filling and chemical interaction between adsorbent and adsorbate is the primary interaction.

References

1. Saleh TA, Mustaqeem M, Khaled M (2022) Water treatment technologies in removing heavy metal ions from wastewater: a review. Environ Nanotechnol Monit Manag 17:100617. https://doi.org/10.1016/J.ENMM.2021.100617

2. Lei Y, Zhang X, Meng X, Wang Z (2022) The preparation of core-shell Fe_3O_4@SiO_2magnetic nanoparticles with different surface carboxyl densities and their application in the removal of methylene blue. Inorg Chem Commun 139:109381. https://doi.org/10.1016/J.INOCHE.2022.109381
3. Tolkou AK, Kyzas GZ, Katsoyiannis IA (2022) Arsenic (V) removal from water sources by molecularly imprinted polymers (MIPs): A mini review of recent developments. Sustainability 14:5222. https://doi.org/10.3390/su14095222
4. Ali MAM, Alsabagh AM, Sabaa MW, El-Salamony RA, Mohamed RR, Morsi RE (2020) Polyacrylamide hybrid nanocomposites hydrogels for efficient water treatment. Iran Polym J 29:455–466. https://doi.org/10.1007/s13726-020-00810-y
5. Vani B, Shivakumar M, Kalyani S, Sridhar S (2021) TiO_2 nanoparticles incorporated high-performance polyphenyl sulfone mixed matrix membranes for ultrafiltration of domestic greywater. Iran Polym J 30:917–934. https://doi.org/10.1007/s13726-021-00945-6
6. Jabbar KQ, Barzinjy AA, Hamad SM (2022) Iron oxide nanoparticles: preparation methods, functions, adsorption and coagulation/flocculation in wastewater treatment. Environ Nanotechnol MonitManag 17:100661. https://doi.org/10.1016/J.ENMM.2022.100661
7. Mallakpour S, Tabesh F (2021) Application of gum polysaccharide nanocomposites in the removal of industrial organic and inorganic pollutants. Handbook Polym Nanocompos Ind Appl 2021:503–528. https://doi.org/10.1016/B978-0-12-821497-8.00018-6
8. Zhao G, Huang X, Tang Z, Huang Q, Niu F, Wang X (2018) Polymer-based nanocomposites for heavy metal ions removal from aqueous solution: a review. Polym Chem 9:3562–3582. https://doi.org/10.1039/C8PY00484F
9. Bassyouni M, Abdel-Aziz MH, Zoromba MS, Abdel-Hamid SM, Drioli E (2019) A review of polymeric nanocomposite membranes for water purification. J Ind Eng Chem 73:19–46. https://doi.org/10.1016/J.JIEC.2019.01.045
10. Saleh TA (2021) Protocols for synthesis of nanomaterials, polymers, and green materials as adsorbents for water treatment technologies. Environ Technol Innov 24:101821. https://doi.org/10.1016/J.ETI.2021.101821
11. Beyene HD, Ambaye TG (2019) Application of sustainable nanocomposites for water purification process. Sustain Polym Compos Nanocompos 2019:387–412
12. Maio A, Gammino M, Gulino EF, Megna B, Fara P, Scaffaro R (2020) Rapid one-step fabrication of graphene oxide-decorated polycaprolactone three-dimensional templates for water treatment. ACS Appl Polym Mater 2020:4993–5005. https://doi.org/10.1021/acsapm.0c00852
13. Li L, Li X, Duan H, Wang X, Luo C (2014) Removal of Congo Red by magnetic mesoporous titanium dioxide–graphene oxide core-shell microspheres for water purification. Dalton Trans 43:8431. https://doi.org/10.1039/c3dt53474j
14. Mallakpour S, Tabesh F (2020) Fabrication technologies of layered double hydroxide polymer nanocomposites. Layered Double Hydroxide Polym Nanocompos 2020:103–155. https://doi.org/10.1016/B978-0-08-101903-0.00003-9
15. Rizvi MA, Moosvi SK, Jan T, Bashir S, Kumar P, Roos WD, Swart HC (2019) Dielectric, magnetic and photocatalytic activity of polypyrrole/Prussian red nanocomposite for waste water treatment applications. Polymer 163:1–12. https://doi.org/10.1016/J.POLYMER.2018.12.044
16. Fan J, Zhang S (2015) Facile preparation of Fe_3O_4/mesoporous TiO_2nanoparticles shell on polystyrene beads and its effective absorption of cyanobacteria in water. J Polym Res 22:182. https://doi.org/10.1007/s10965-015-0818-z
17. Arumugam V, Redhi GG, Gengan RM (2016) Efficient catalytic activity of ionic liquid-supported $NiFe_2O_4$ magnetic nanoparticle doped titanium dioxide nano-composite. Int J Chem Eng Appl 7:422–427 https://doi.org/10.18178/ijcea.2016.7.6.618
18. Valamohammadi E, Behdarvand F, Mohammadi T, Tofighy MA, Moghiseh Z (2022) Effects of carbon nanotubes on structure, performance and properties of polymer nanocomposite membranes for water/wastewater treatment applications: a comprehensive review. Polym Bull 18:1–44. https://doi.org/10.1007/s00289-022-04635-y
19. Saleh TA, Parthasarathy P, Irfan M (2019) Advanced functional polymer nanocomposites and their use in water ultra-purification. Trends Environ Anal Chem 24:e00067. https://doi.org/10.1016/J.TEAC.2019.E00067
20. Abdollahi H, Ershad-Langroudi A, Salimi A, Rahimi A (2014) Anticorrosive coatings prepared using epoxy-silica hybrid nanocomposite materials. Ind Eng Chem Res 53:10858–10869. https://doi.org/10.1021/ie501289g
21. Kumar M, Dosanjh HS, Singh J, Monir K, Singh H (2020) Review on magnetic nanoferrites and their composites as alternatives in waste water treatment: synthesis, modifications and applications. Environ Sci 6:491–514. https://doi.org/10.1039/C9EW00858F
22. Pazokifard S, Farrokhpay S, Mirabedini M, Esfandeh M (2015) Surface treatment of TiO_2 nanoparticles via sol-gel method: effect of silane type on hydrophobicity of the nanoparticles. Prog Org Coat 87:36–44. https://doi.org/10.1016/J.PORGCOAT.2015.04.021
23. Abid M, Ben Haj Amara A, Bechelany M (2023) Halloysite-TiO_2 nanocomposites for water treatment: a review. Nanomaterials 13:1578. https://doi.org/10.3390/nano13091578
24. Alsaiari NS, Amari A, Katubi KM, Alzahrani FM, Rebah FB, Tahoon MA (2021) Innovative magnetite based polymeric nanocomposite for simultaneous removal of methyl orange and hexavalent chromium from water. Processes 9:576. https://doi.org/10.3390/pr9040576
25. Acharya R, Lenka A, Parida K (2021) Magnetite modified amino group based polymer nanocomposites towards efficient adsorptive detoxification of aqueous Cr (VI): a review. J Mol Liq 337:116487. https://doi.org/10.1016/J.MOLLIQ.2021.116487
26. Mudassir MA, Hussain SZ, Jilani A, Zhang H, Ansari TM, Hussain I (2019) Magnetic hierarchically macroporous emulsion-templated poly (acrylic acid)–iron oxide nanocomposite beads for water remediation. Langmuir 35:8996–9003. https://doi.org/10.1021/acs.langmuir.9b01121
27. Ali I (2012) New generation adsorbents for water treatment. Chem Rev 112:5073–5091. https://doi.org/10.1021/cr300133d
28. Falciglia PP, Gagliano E, Scandura P, Bianco C, Tosco T, Sethi R, Varvaro G, Agostinelli E, Bongiorno C, Russo A, Romano S (2022) Physico-magnetic properties and dynamics of magnetite (Fe_3O_4) nanoparticles (MNPs) under the effect of permanent magnetic fields in contaminated water treatment applications. Sep Purif Technol 296:121342. https://doi.org/10.1016/J.SEPPUR.2022.121342
29. Zhang Q, Lu D, Wang D, Yang X, Zuo P, Yang H, Fu Q, Liu Q, Jiang G (2020) Separation and tracing of anthropogenic magnetite nanoparticles in the urban atmosphere. Environ Sci Technol 54:9274–9284. https://doi.org/10.1021/acs.est.0c01841
30. Sosun AA, Mannan A, Ali Shah U, Zia M (2022) Removal of toxic metal ions (Ni^{2+} and Cd^{2+}) from wastewater by using TOPO decorated iron oxide nanoparticles. Appl Water Sci 12:86. https://doi.org/10.1007/s13201-022-01588-5
31. Hong J, Xie J, Mirshahghassemi S, Lead J (2020) Metal (Cd, Cr, Ni, Pb) removal from environmentally relevant waters using polyvinylpyrrolidone-coated magnetite nanoparticles. RSC Adv 10:3266–3276. https://doi.org/10.1039/C9RA10104G
32. Mohammadi A, Barikani M, Barmar M (2013) Effect of surface modification of Fe_3O_4 nanoparticles on thermal and mechanical properties of magnetic polyurethane elastomer

nanocomposites. J Mater Sci 48:7493–7502. https://doi.org/10.1007/s10853-013-7563-7
33. Samrot AV, Sahithya CS, Selvarani J, Purayil SK, Ponnaiah P (2021) A review on synthesis, characterization and potential biological applications of superparamagnetic iron oxide nanoparticles. Current Res Green Sustain Chem 4:100042. https://doi.org/10.1016/J.CRGSC.2020.100042
34. Bustamante-Torres M, Romero-Fierro D, Estrella-Nuñez J, Arcentales-Vera B, Chichande-Proaño E, Bucio E (2022) Polymeric composite of magnetite iron oxide nanoparticles and their application in biomedicine: a review. Polymers 14:752. https://doi.org/10.3390/polym14040752
35. Roca AG, Gutiérrez L, Gavilán H, Brollo ME, Veintemillas-Verdaguer S, del Puerto MM (2019) Design strategies for shape-controlled magnetic iron oxide nanoparticles. Adv Drug Deliv Rev 138:68–104. https://doi.org/10.1016/J.ADDR.2018.12.008
36. Raza M, Bachinger A, Zahn N, Kickelbick G (2014) Interaction and UV-stability of various organic capping agents on the surface of anatase nanoparticles. Materials 7:2890–2912. https://doi.org/10.3390/ma7042890
37. Salman D, Juzsakova T, Al-Mayyahi MA, Ákos R, Mohsen S, Ibrahim RI, Mohammed HD, Abdullah TA, Domokos E, Korim T (2021) Synthesis, surface modification and characterization of magnetic Fe_3O_4@ SiO_2 core-shell nanoparticles. J Phys Conf Ser 1773:012039. https://doi.org/10.1088/1742-6596/1773/1/012039
38. Liu S, Yu B, Wang S, Shen Y, Cong H (2020) Preparation, surface functionalization and application of Fe3O4 magnetic nanoparticles. Adv Colloid Interface Sci 281:102165. https://doi.org/10.1016/J.CIS.2020.102165
39. Wang Y, Gu H (2015) Core-shell-type magnetic mesoporous silica nanocomposites for bioimaging and therapeutic agent delivery. Adv Mater 27:576–585. https://doi.org/10.1002/adma.201401124
40. Bhateria R, Singh R (2019) A review on nanotechnological application of magnetic iron oxides for heavy metal removal. J Water Proc Eng 31:100845. https://doi.org/10.1016/J.JWPE.2019.100845
41. Cheng JP, Ma R, Li M, Wu JS, Liu F, Zhang XB (2012) Anatase nanocrystals coating on silica-coated magnetite: role of polyacrylic acid treatment and its photocatalytic properties. Chem Eng J 210:80–86. https://doi.org/10.1016/J.CEJ.2012.08.059
42. Jacinto MJ, Ferreira LF, Silva VC (2020) Magnetic materials for photocatalytic applications: a review. J Solgel Sci Technol 96:1–14. https://doi.org/10.1007/s10971-020-05333-9
43. Ershad-Langroudi A, Rabiee A (2012) A novel acrylamide-anatase hybrid nanocomposite. J Polym Res 19:9970. https://doi.org/10.1007/s10965-012-9970-x
44. Sadiaa M, Saqiba A, Khana J, Zahoorb M, Zekkerc I (2022) Photocatalytic degradation of methyl orange and toluidine blue using advanced oxidation method. Desalin Water Treat 262:256–265. https://doi.org/10.5004/dwt.2022.28554
45. Inturi SNR, Boningari T, Suidan M, Smirniotis PG (2014) Visible-light-induced photodegradation of gas phase acetonitrile using aerosol-made transition metal (V, Cr, Fe Co, Mn, Mo, Ni, Cu, Y, Ce, and Zr) doped TiO2. Appl Catal B 144:333–342. https://doi.org/10.1016/j.apcatb.2013.07.032
46. Rabiee A, Ershad-Langroudi A, Zeynali ME (2015) A survey on cationic polyelectrolytes and their applications: acrylamide derivatives. Rev Chem Eng 31:56. https://doi.org/10.1515/revce-2014-0056
47. Maćczak P, Kaczmarek H, Ziegler-Borowska M (2020) Recent achievements in polymer bio-based flocculants for water treatment. Materials 13:3951. https://doi.org/10.3390/ma13183951
48. Pashapouryeganeh F, Zargar G, Rabiee A, Kadkhodaie A, Takassi MA (2022) Design and synthesis of cationic copolymer synergized with metal nanoparticles as polymeric hybrid nanocomposite for carbonate reservoir applications. Polym Bull 80:7865–7882. https://doi.org/10.1007/s00289-022-04405-w
49. Kokate M, Garadkar K, Gole A (2013) One pot synthesis of magnetite-silica nanocomposites: applications as tags, entrapment matrix and in water purification. J Mater Chem A 1:2022–2029. https://doi.org/10.1039/C2TA00951J
50. Jain R (2022) Recent advances of magnetite nanomaterials to remove arsenic from water. RSC Adv 12:32197–32209. https://doi.org/10.1039/D2RA05832D
51. Wang C, Yin L, Zhang L, Kang L, Wang X, Gao R (2009) Magnetic $(\gamma\text{-}Fe_2O_3@SiO_2)_n@TiO_2$ functional hybrid nanoparticles with activated photocatalytic ability. J Phys Chem C 113:4008–4011. https://doi.org/10.1021/jp809835a
52. Shchukin DG, Ustinovich EA, Sviridov DV, Kulak AI (2004) Titanium and iron oxide-based magnetic photocatalysts for oxidation of organic compounds and sulfur dioxide. High Energy Chem 38:167–173. https://doi.org/10.1023/B:HIEC.0000027654.45001.00
53. Khoo YS, Lau WJ, Liang YY, Karaman M, Gürsoy M, Ismail AF (2022) Eco-friendly surface modification approach to develop thin film nanocomposite membrane with improved desalination and antifouling properties. J Adv Res 36:39–49. https://doi.org/10.1016/j.jare.2021.06.011
54. Fonseca FV, Silva LLS, Linhares AMF, Borges CP (2023) Current trends of nano-enhanced polymeric membranes for water and wastewater reclamation. Novel Mater Environ Remed Appl 2023:63–98. https://doi.org/10.1016/B978-0-323-91894-7.00018-9
55. Dadpanah A, Rabiee A, Mohammadi F, ErshadLangroudi A, Zeynali ME (2022) Preparation and characterization of AM-*co*-APTAC/TiO_2nanocomposite for environmental applications. Polym Bull 79:1039–1055. https://doi.org/10.1007/s00289-020-03512-w
56. Ashraf S, Siddiqa A, Shahida S, Qaisar S (2019) Titanium-based nanocomposite materials for arsenic removal from water: a review. Heliyon 5:e01577. https://doi.org/10.1016/j.heliyon.2019.e01577
57. Xu J, Ju C, Sheng J, Wang F, Zhang Q, Sun G, Sun M (2013) Synthesis and characterization of magnetic nanoparticles and its application in lipase immobilization. Bull Korean Chem Soc 34:2408–2412. https://doi.org/10.5012/bkcs.2013.34.8.2408
58. Kittappa S, Pichiah S, Kim JR, Yoon Y, Snyder SA, Jang M (2015) Magnetised nanocomposite mesoporous silica and its application for effective removal of methylene blue from aqueous solution. Sep Purif Technol 153:67–75. https://doi.org/10.1016/J.SEPPUR.2015.08.019
59. Yang N, Luo ZX, Chen SC, Wu G, Wang YZ (2020) Fe_3O_4 nanoparticle/N-doped carbon hierarchically hollow microspheres for broadband and high-performance microwave absorption at an ultralow filler loading. ACS Appl Mater Interfaces 12:18952–18963. https://doi.org/10.1021/acsami.0c04185
60. Asab G, Zereffa EA, AbdoSeghne T (2020) Synthesis of silica-coated Fe_3O_4 nanoparticles by microemulsion method: characterization and evaluation of antimicrobial activity. Int J Biomater 2020:1–11. https://doi.org/10.1155/2020/4783612
61. Yuan Q, Li N, Geng W, Chi Y, Li X (2012) Preparation of magnetically recoverable Fe_3O_4@SiO_2@meso-TiO_2nanocomposites with enhanced photocatalytic ability. Mater Res Bull 47:2396–2402. https://doi.org/10.1016/j.materresbull.2012.05.031
62. Absalan F, Nikazar M (2016) Application of response surface methodology for optimization of water treatment by Fe_3O_4 / SiO_2 /TiO_2 core-shell nano-photocatalyst. Chem Eng Commun 203:1523–1531. https://doi.org/10.1080/00986445.2016.1218335
63. Mousavi SE, Younesi H, Bahramifar N, Tamunaidu P, Karimi-Maleh H (2022) A novel route to the synthesis of α-Fe_3O_4/SiO_2/TiO_2 nanocomposite from the metal-organic framework as a

photocatalyst for water treatment. Chemosphere 297:133992. https://doi.org/10.1016/j.chemosphere.2022.133992
64. Corredor LM, Husein MM, Maini BB (2019) Impact of PAM-grafted nanoparticles on the performance of hydrolyzed polyacrylamide solutions for heavy oil recovery at different salinities. Ind Eng Chem Res 58:9888–9899. https://doi.org/10.1021/acs.iecr.9b01290
65. Wang H, Chao L, Wei X, Li J, Ji C, Wang B, Qi X, Hu P, Ying Y, Tian M (2019) Design of SiO_2-TiO_2-PAM composite flocculant with self-degrading characteristics and optimization of the flocculation process using a combination of central composite design and response surface methodology. Colloids Surf A Physicochem Eng Asp 583:123982. https://doi.org/10.1016/j.colsurfa.2019.123982
66. Mallakpour S, Abdolmaleki A, Tabesh F (2018) Ultrasonic-assisted manufacturing of new hydrogel nanocomposite biosorbent containing calcium carbonate nanoparticles and tragacanth gum for removal of heavy metal. Ultrason Sonochem 41:572–581. https://doi.org/10.1016/j.ultsonch.2017.10.022
67. Dada AO, Olalekan AP, Olatunya AM, Dada OJ (2012) Langmuir, Freundlich, Temkin and Dubinin-Radushkevich isotherms studies of equilibrium sorption of Zn^{2+} unto phosphoric acid modified rice husk. IOSR J Appl Chem 3:38–45. https://doi.org/10.9790/5736-0313845
68. Mallakpour S, Tabesh F (2019) Tragacanth gum based hydrogel nanocomposites for the adsorption of methylene blue: Comparison of linear and non-linear forms of different adsorption isotherm and kinetics models. Int J Biol Macromol 133:754–766. https://doi.org/10.1016/j.ijbiomac.2019.04.129
69. Brion-Roby R, Gagnon J, Deschênes JS, Chabot B (2018) Development and treatment procedure of arsenic-contaminated water using a new and green chitosan sorbent: kinetic, isotherm, thermodynamic and dynamic studies. Pure Appl Chem 90:63–77. https://doi.org/10.1515/pac-2017-0305